Supporting Information for

Multifunctional hybrid porous filters with hierarchical structures for simultaneous removal of indoor VOCs, dusts and microorganisms

Yang Zhao,[a] Ze-Xian Low,[b] Shasha Feng,[a] Zhaoxiang Zhong,*[,a] Yong Wang,[a] Zhong Yao,[a]

[a]State Key Laboratory of Materials-Oriented Chemical Engineering, National Engineering Research Center for Special Separation Membrane, Nanjing Tech University, Nanjing 210009, China
E-mail: njutzzx@163.com (Z. Z.)
[b]Dr. Z. Low
Centre for Advanced Separations Engineering and Department of Chemical Engineering, University of Bath, Claverton Down, Bath BA2 7AY, United Kingdom

Table of Content

1. Chemical Vapour Deposition of MWCNTs onto Al_2O_3 filters

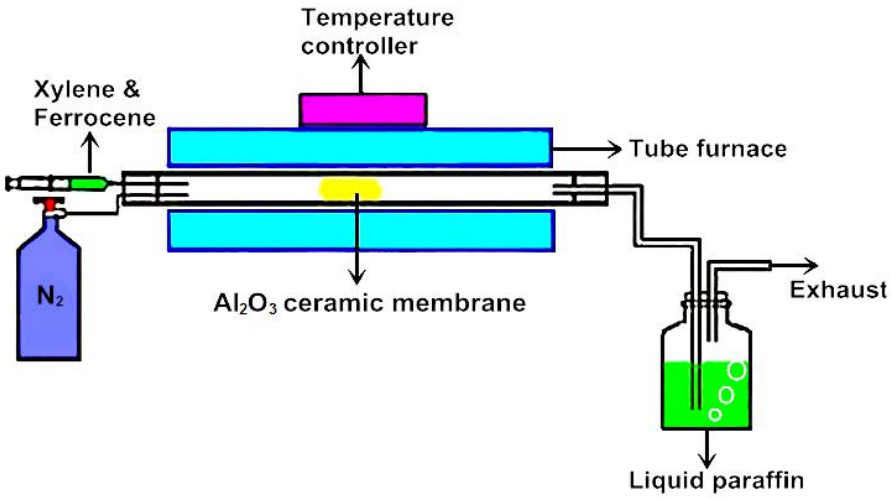

Figure S1. Schematic representation of chemical vapour deposition (CVD) of MWCNTs on Al_2O_3 ceramic membrane. N_2 was used as the carrier and protective gas. Xylene and ferrocene were used for carbon source and catalyst for MWCNTs growth. Liquid paraffin was used for the removal of residue xylene and ferrocene in the exhaust.

2. Dynamic filtration experiment and bacterial culture preparation

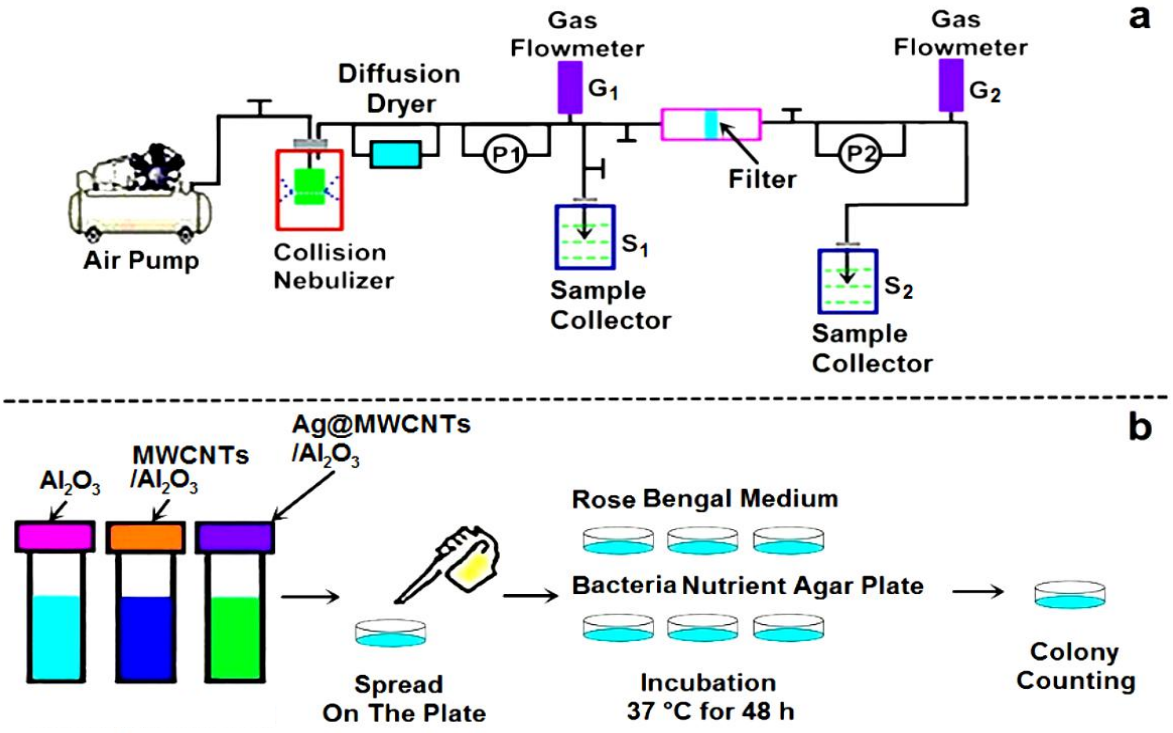

Figure S2. Schematic representation of the dynamic experimental procedure of the retainment of the aerosol microorganisms (a) and the antimicrobic test for the microorganisms retained on the filters after filtration (b). *Escherichia coli* (*E. coli*, ATCC 25922), Bacillus subtilis (*B. subtilis,* ATCC 6051) and Aspergillus niger (*A. niger,* ATCC 16404) were selected as the model Gram-negative bacteria, Gram-positive bacteria and fungi to test the antimicrobial properties of the filters.

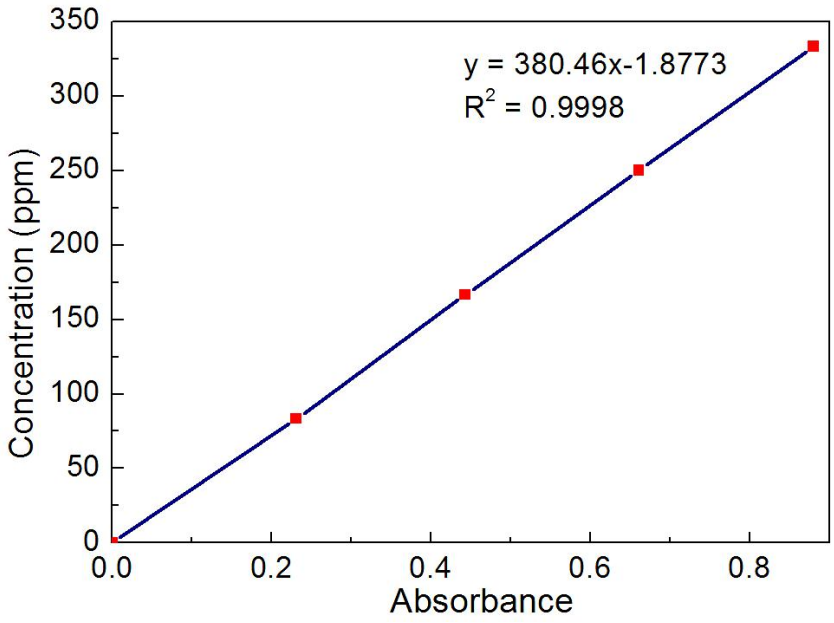

Figure S3. Standard calibration curve of formaldehyde concentration.

3. Aerosol filtration experiment

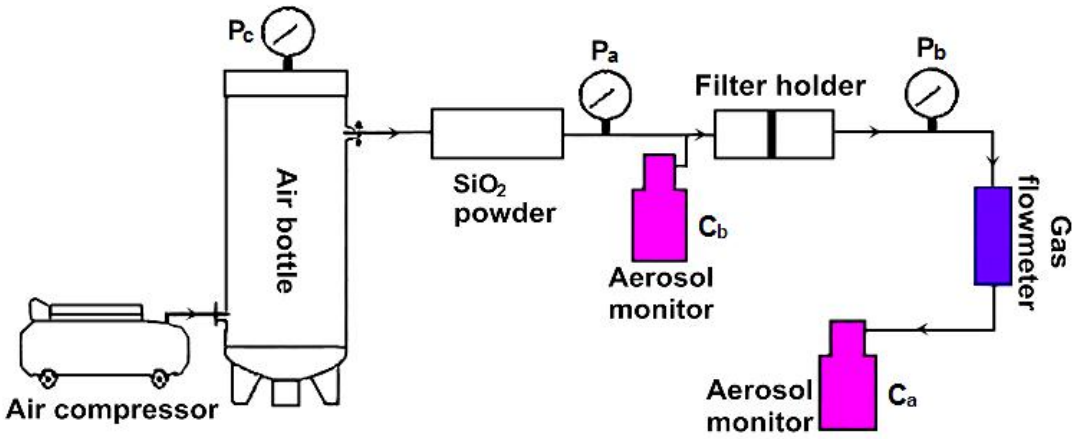

Figure S4. Schematic representation for the removal of aerosol particles test. P_c is the pressure of the air bottle, while P_a is the pressure before the filter holder, and P_b is the pressure after the filter holder. C_b and C_a refer to the concentration of SiO_2 particles before and after the filtration, respectively.

4. SEM analysis of Al_2O_3, MWCNTs/Al_2O_3 and Ag@MWCNTs/Al_2O_3 filters

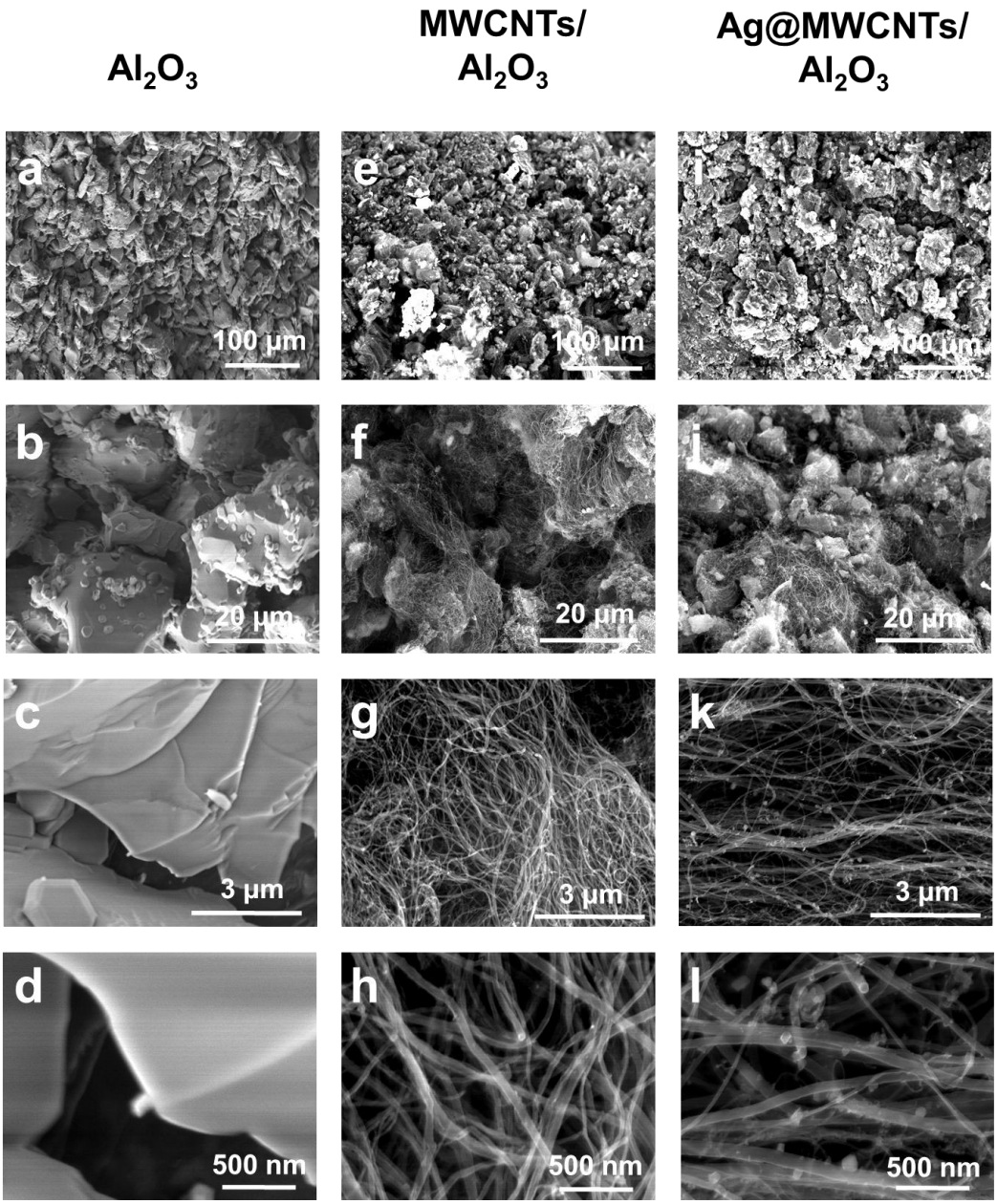

Figure S5. Surface morphology of (a-d) Al_2O_3, (e-h) MWCNTs/Al_2O_3, and (i-l) Ag@MWCNTs/Al_2O_3 at different magnification.

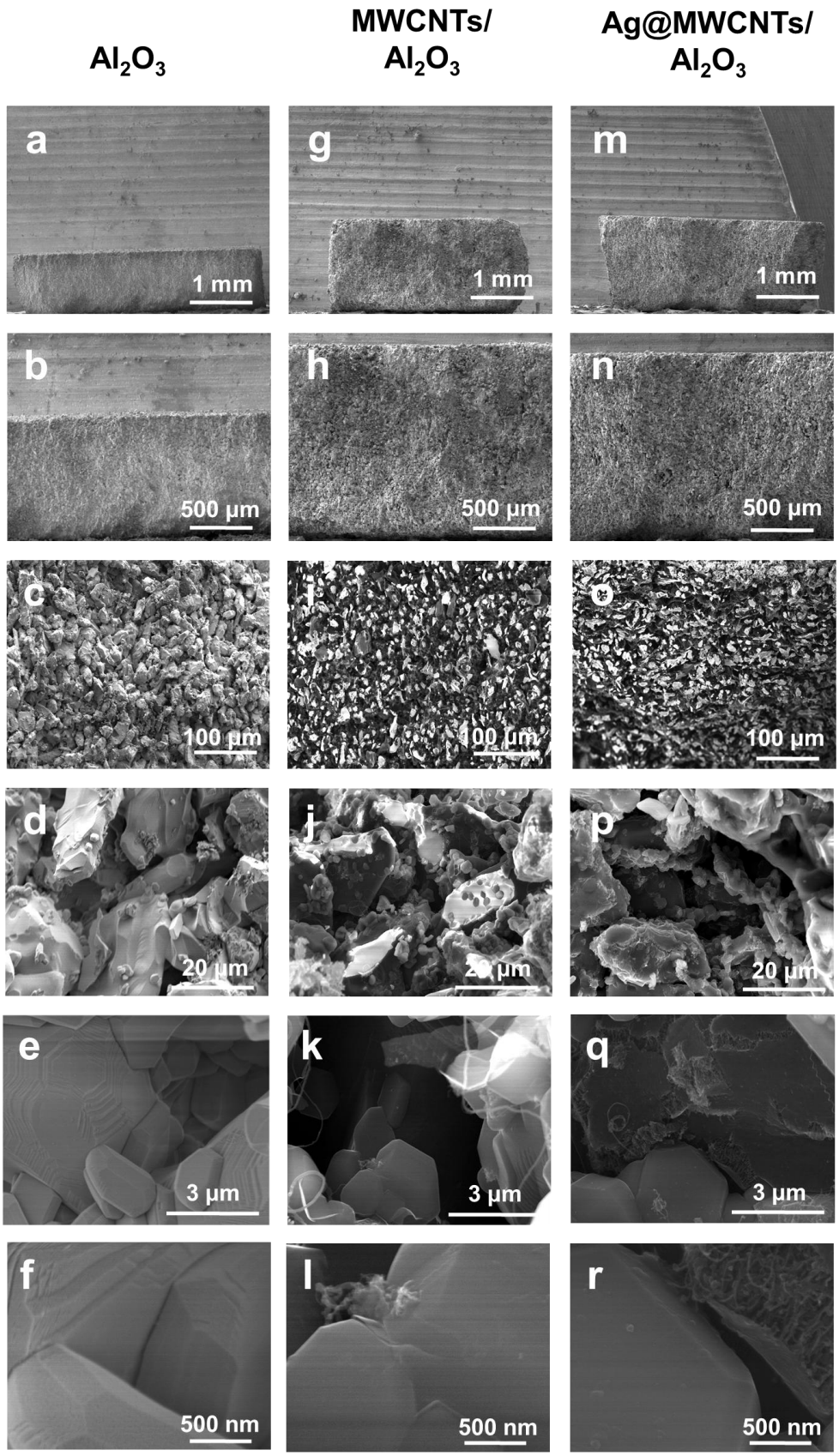

Figure S6. Cross sectional morphology of (a-f) Al_2O_3, (g-l) MWCNTs/Al_2O_3, and (m-r) Ag@MWCNTs/Al_2O_3 at different magnification.

5. X-ray diffraction spectroscopy of Al_2O_3, MWCNTs/Al_2O_3 and Ag@MWCNTs/Al_2O_3 filters

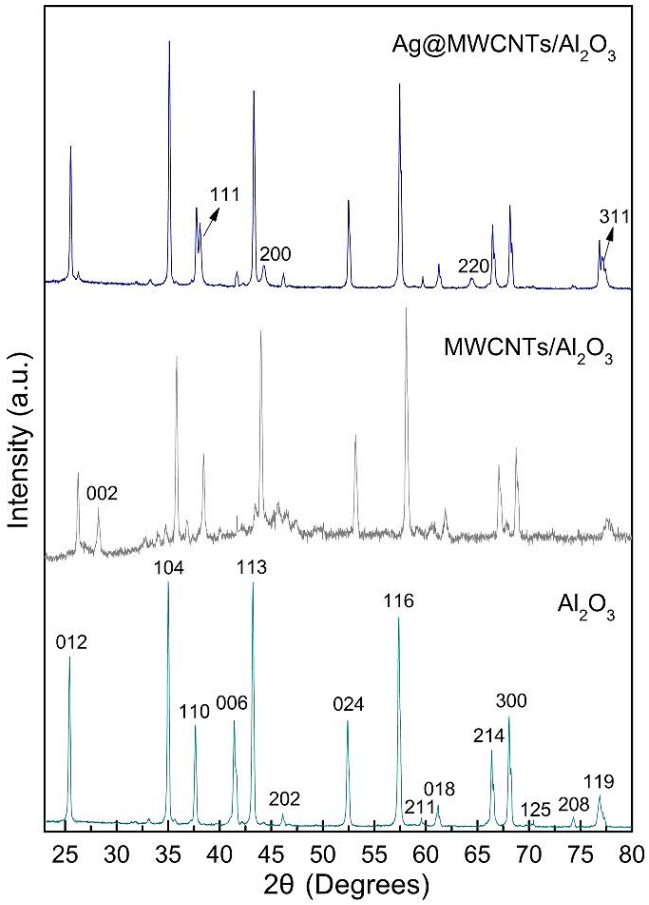

Figure S7. XRD pattern of the Ag@MWCNTs/Al_2O_3, MWCNTs/Al_2O_3 and Al_2O_3 filter.

XRD measurement was performed to investigate the crystallographic structures of the filter samples as showed in **Figure S7**. For the XRD measurement of Ag@MWCNTs/Al_2O_3 hybrid filter, four peaks located at 38.12º, 44.3º, 64.4º and 77.5º were assigned to the diffraction line of the (111), (200), (220), (311) crystalline planes of the metallic silver, respectively (JCPDS 04-0783). The characteristic peaks of the Al_2O_3 filter correspond to the corundum Al_2O_3 (JCPDS 46-1212), indicating that the dominating content of the matrix of the MWCNTs/Al_2O_3 hybrid filter and the Ag@MWCNTs/Al_2O_3 hybrid filter was corundum Al_2O_3. The presence of the (002) peak at 26.5º indicates that the MWCNTs grown on the Al_2O_3 matrix were not well-aligned and the MWCNTs were intertwined with each other forming a "network-like" hierarchical structure.[1]

6. Mixed acid treatments of MWCNTs

Before the loading of AgNPs, the MWCNTs grown on Al_2O_3 membrane were treated by the mixed acid solution of HCl, HNO_3 and H_2SO_4 to improve the surface activity of the MWCNTs through the rupture of carbon-to-carbon bond and introduction of oxygenated functional groups.[1-2] The infrared spectra of the MWCNTs/Al_2O_3 hybrid filter before and after the mixed acid treatment are represented in **Figure S8a**. The incidence of 3430 cm^{-1} band is attributed to the presence of hydroxyl (-OH) groups connected to the surface of the MWCNTs, and the new peak at 1720 cm^{-1} is caused by the formation of carboxyl (-COOH). The -COOH groups increase the hydrophilicity of the MWCNTs which improves the homogeneous attachment of the AgNPs during the polyol process. A_{2u} modes and E_{1u} modes are the main active modes of MWCNTs peaked at 860 and 1580 cm^{-1}, respectively, which appear in all CNTs and are independent of the diameters.[1] Consequently, the functional groups introduced on the surface of the MWCNTs causes the filter sample to absorb carbon dioxide from the air, leading to the influence of background and peaked at 2350 cm^{-1} in the FT-IR spectra image.

The Raman spectrum of the CNTs scraped from the MWCNTs/Al_2O_3 hybrid filter before and after acid treatment is represented in **Figure S8b**. Three characteristic peaks around 1340 cm^{-1} D-band, 1550 cm^{-1} G-band, and 2650 cm^{-1} G'-band of MWCNTs confirmed the growth of MWCNTs.[33] D-band represents the structural imperfections and impurities of MWCNTs and assigned to Raman mode of the amorphous carbon, while G-band contributes to the tangential radial mode of graphite. G'-band is assigned to the first overtone of the D-band.[3] For the line after acid treatment in **Figure S8b**, the quotient for the Raman intensity of D-band and G-band (I_D /I_G) is 0.68, which is higher than the line before acid treatment 0.54, indicating that the mixed acid causes the opening of the caps which break the MWCNTs, creating more deficiencies.[4] **Figure S8c** illustrates that the acid treatment and compression effect caused by the AgNPs on MWCNTs though the polyol process may be responsible for the deformation of the MWCNTs, and in line with the

TEM results presented in the main text.

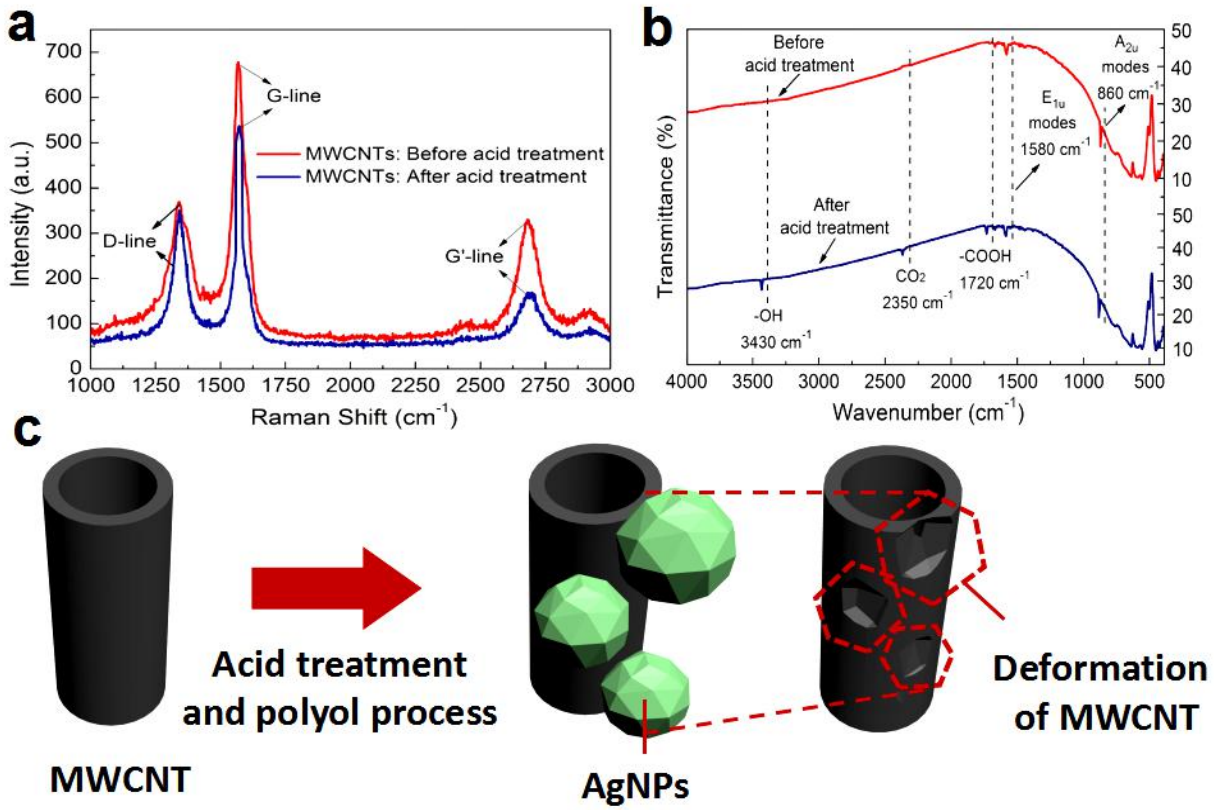

Figure S8. (a) FT-IR spectra for the MWCNTs/Al_2O_3 hybrid filter before and after the mixed acid treatment, (b) Raman spectrum of the MWCNTs on the MWCNTs/Al_2O_3 hybrid filter before and after acid treatment, and (c) deformation of the MWCNTs caused by the acid treatment and polyol process.

7. Specific surface area of Al_2O_3, MWCNTs/Al_2O_3 and Ag@MWCNTs/Al_2O_3 filters

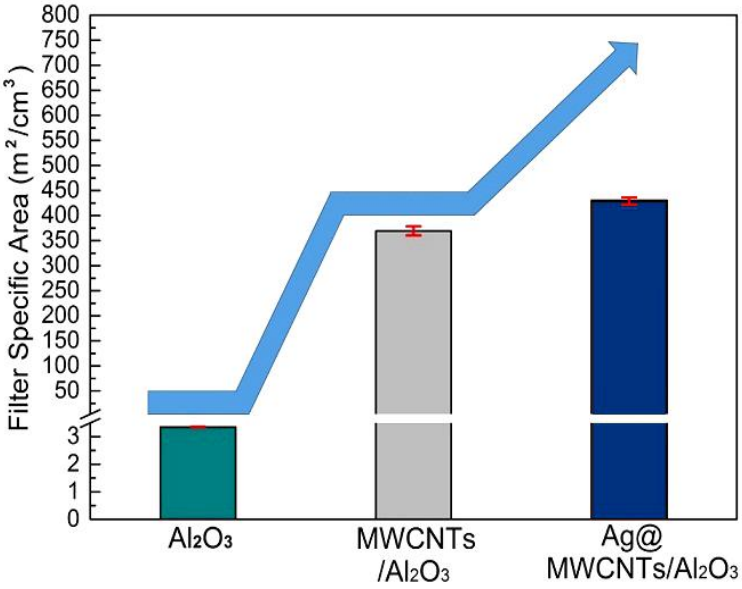

Figure S9. the specific area of the filters.

Filter specific area (m^2/cm^3) was determined based on the volume of the filters rather the mass of the filters to determine the improvement to the surface area packed into the same volume of a final filtration system. It can be observed that as much as ~126.14 times improvement of specific area was achieved by incorporating Ag@MWCNTs in a Al_2O_3 filter.

8. Mechanical Stability Test

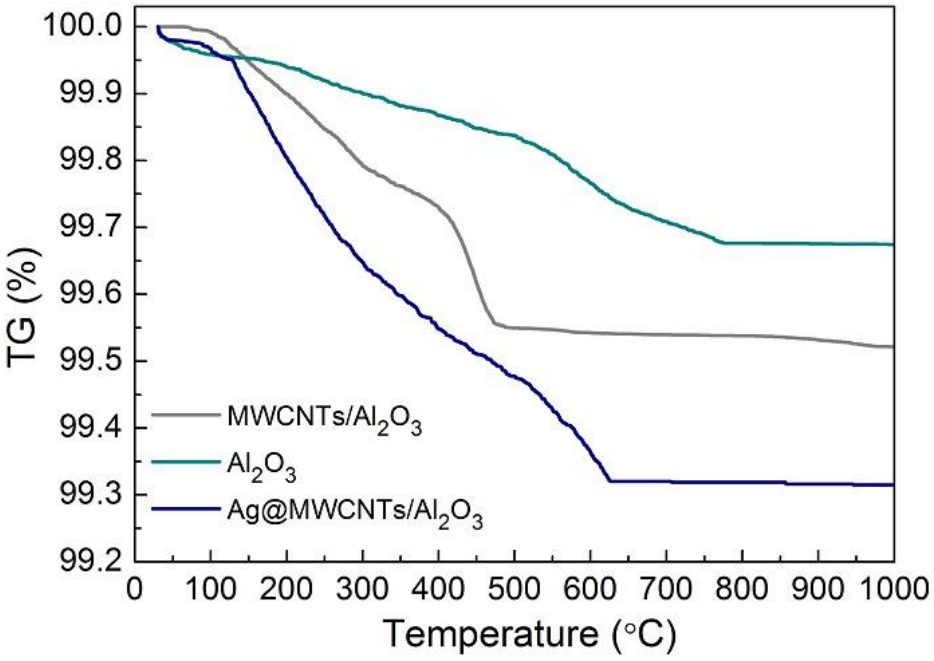

Figure S10. Thermogravimetric analysis of Al_2O_3, MWCNTs/Al_2O_3 and Ag@MWCNTs/Al_2O_3 filters.

Figure S10 shows the thermograms of the filters. The filters showed high thermal stability with a negligible mass loss of 0.7 %, 0.48 % and 0.32 % for the Ag@MWCNTs/Al_2O_3 hybrid filter, MWCNTs/Al_2O_3 hybrid filter and Al_2O_3 filter, respectively within 1000 °C due to the strong thermal stability materials of Al_2O_3 matrix and metal silver. The initial mass loss of the filters around 100 – 150 °C can be ascribed to the evaporation of the water from the ambient moisture. Beyond 100 °C, continuous mass loss is observed in all samples due to removal of absorbed carbonaceous particles. Higher amount of mass loss is observed for MWCNTs/Al_2O_3 hybrid filter and Ag@MWCNTs/ Al_2O_3 hybrid filter due to the additional removal of the amorphous carbon in the MWCNTs. After incorporation of the AgNPs, the Ag@MWCNTs/Al_2O_3 hybrid filter showed decomposition at a lower temperature as the metal silver is an oxidative catalyst for accelerating the thermal decomposition of MWCNTs in air atmosphere.[4-5]

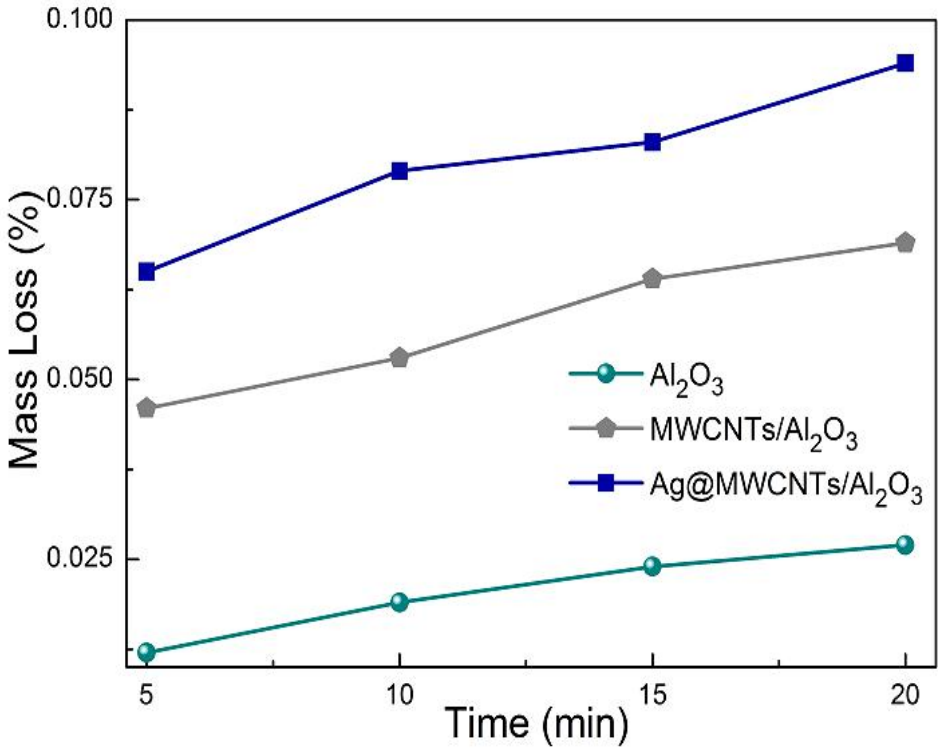

Figure S11. Mass loss of the filters as a function of ultrasonication time.

The mechanical stability test of the filters is shown in **Figure S11**. The mass of the filters decreased with the increasing ultrasonication time. Similar to the TG results, the Al_2O_3 filter shows the highest mechanical stability with a mass loss of 0.03 %, followed by the MWCNTs/Al_2O_3 hybrid filter (0.07 %) and the Ag@MWCNTs/Al_2O_3 hybrid filter (0.09 %) at the ultrasonication time of 20 min. The original stability of the filters (Al_2O_3) and the stable electrostatic attraction between the surface of MWCNTs and AgNPs could be mainly responsible for the mechanical stability of Ag@MWCNTs/Al_2O_3 hybrid filter, and these results indicated that the polyol process produced a highly thermal and mechanical stabilized Ag@MWCNTs/Al_2O_3 hybrid filter.

9. Digital image of microbial culture

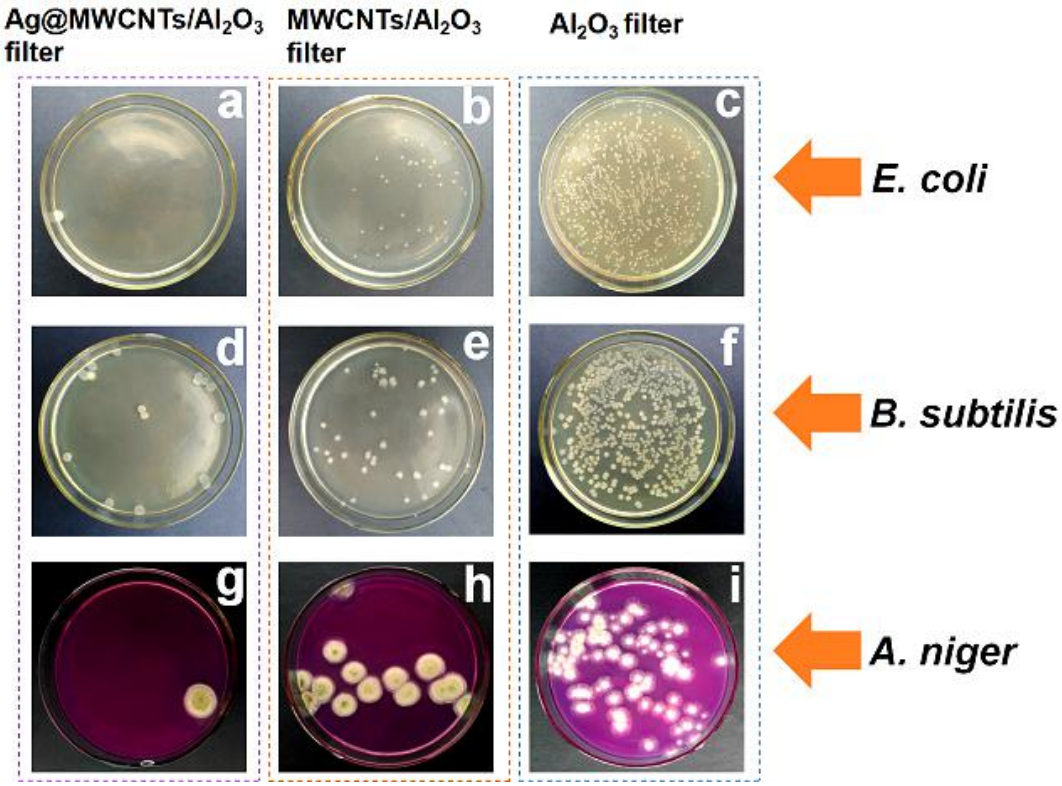

Figure S12. Antimicrobic efficacy of aerosol microorganisms on the filters after the dynamic retention test. (a)-(c): *E.coli*, (d)-(f): *B.subtilis*, (g)-(i): *A.niger*, antimicrobic rate tested by the Ag@MWCNTs/Al_2O_3 (a, d, g), MWCNTs/ Al_2O_3 (b, e, h) and Al_2O_3 filters (c, f, i) respectively.

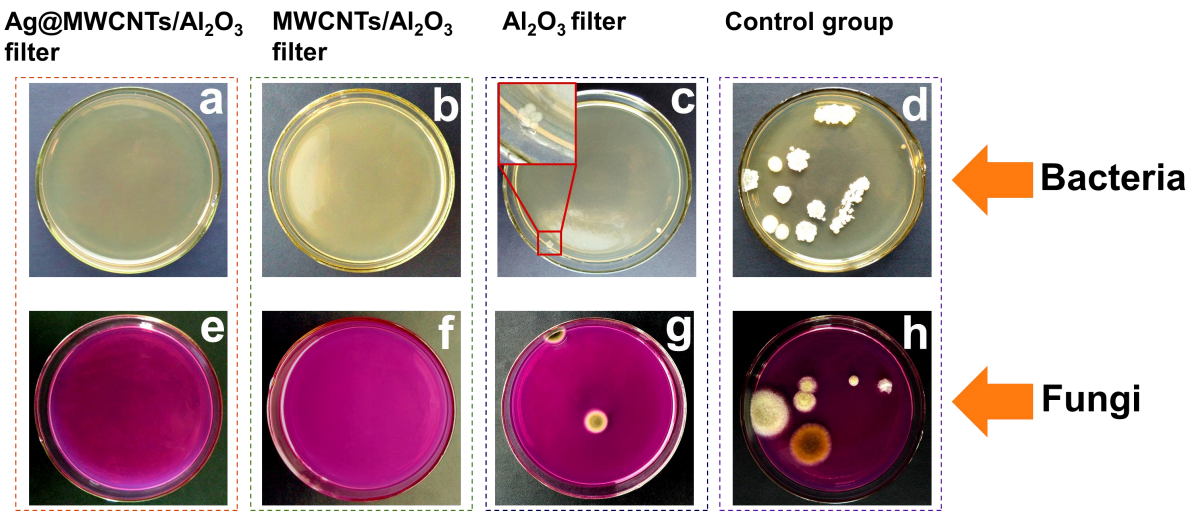

Figure S13. Dynamic retention test of the filters for the practical atmospheric environment. (d) and (h) were the control group. (a)-(d) and (e)-(h) represented LB nutrient agar group and rose bengal medium group, respectively as tested by the Ag@MWCNTs/Al_2O_3 (a,e), MWCNTs/Al_2O_3 (b,f) and Al_2O_3 filter (c,g).

10. Formaldehyde degradation performance comparison

Table S1. Date of pore diameter of the filters.

Al_2O_3		MWCNTs/Al_2O_3		Ag@MWCNTs/Al_2O_3	
Pore Diameter (μm)	Percentage (%)	Pore Diameter (μm)	Percentage (%)	Pore Diameter (μm)	Percentage (%)
3.86	0.017±0.001	3.78	0.018±0.001	3.571	0.132±0.007
3.8	0.408±0.020	3.7	0.563±0.028	3.5	3.213±0.161
3.7	0.591±0.030	3.6	0.703±0.035	3.4	4.526±0.226
3.6	0.653±0.033	3.5	1.033±0.052	3.3	4.611±0.231
3.5	1.045±0.052	3.4	1.285±0.064	3.2	6.028±0.301
3.4	7.82±0.391	3.3	1.781±0.089	3.1	7.845±0.392
3.3	64.47±3.224	3.2	2.108±0.105	3	8.165±0.408
3.2	12.274±0.614	3.1	2.022±0.101	2.9	8.542±0.427
3.1	9.58±0.479	3	51.653±2.583	2.8	9.804±0.490
3	0±0.000	2.9	33.884±1.694	2.7	10.97±0.545
2.9	1.55±0.078	2.8	0.081±0.004	2.6	11.683±0.591
2.8	0±0.000	2.7	0.08±0.004	2.5	13.914±0.698
2.7	0±0.000	2.6	0.08±0.004	2.4	9.265±0.463
2.6	0.002±0.000	2.5	0.08±0.004	2.3	1.149±0.057
2.5	0.003±0.000	2.4	0.167±0.008	2.2	0.12±0.001
2.4	0.003±0.000	2.3	0.287±0.014	2.1	0.018±0.001
2.3	0.003±0.000	2.2	0.287±0.014	2	0.015±0.001
2.2	0.168±0.008	2.1	0.288±0.014	1.9	0±0.000
2.1	0.189±0.009	2	0.298±0.015	1.8	0±0.000
2	0.184±0.009	1.9	0.298±0.015	1.7	0±0.000
1.9	0.161±0.008	1.8	0.431±0.022	1.6	0±0.000
1.8	0.166±0.008	1.7	0.481±0.024	1.5	0±0.000
1.7	0.205±0.010	1.6	0.628±0.031	1.4	0±0.000

1.6	0.265±0.013	1.5	0.958±0.048	–	–
1.53	0.243±0.012	1.456	0.506±0.025	–	–

Table S2. Date of distribution and N_2 flow-rate of the filters.

Al_2O_3		MWCNTs/Al_2O_3		Ag@MWCNTs/Al_2O_3	
Pressure (kPa)	Flow-rate ($m^3/m^2.h$)	Pressure (kPa)	Flow-rate ($m^3/m^2.h$)	Pressure (kPa)	Flow-rate ($m^3/m^2.h$)
0	0±0.0	0	0±0.0	–	–
0.648	150±7.5	0.629	150±7.5	–	–
1.278	300±15.0	1.24	300±15.0	0.629	150±7.5
1.888	450±22.5	1.774	450±22.5	1.24	300±15.0
2.46	600±30.0	2.308	600±30.0	1.85	450±22.5
3.033	750±37.5	2.88	750±37.5	2.365	600±30.0
3.662	900±45.0	3.529	900±45.0	2.975	750±37.5
4.253	1050±52.5	4.063	1050±52.5	3.605	900±45.0
4.826	1200±60.0	4.635	1200±60.0	4.177	1050±52.5
5.417	1350±67.5	5.188	1350±67.5	4.749	1200±60.0
5.97	1500±75.0	5.741	1500±75.0	5.302	1350±67.5
6.58	1650±82.5	6.294	1650±82.5	5.875	1500±75.0
7.133	1800±90.0	6.828	1800±90.0	6.447	1650±82.5
7.706	1950±97.5	7.381	1950±97.5	6.981	1800±90.0
8.316	2100±105.0	7.973	2100±105.0	7.572	1950±97.5
8.888	2250±112.5	8.545	2250±112.5	8.202	2100±105.0
9.422	2400±120.0	9.098	2400±120.0	8.774	2250±112.5
9.975	2550±127.5	9.651	2550±127.5	9.308	2400±120.0
10.567	2700±135.0	10.185	2700±135.0	9.899	2550±127.5

11.101	2850±142.5	10.719	2850±142.5	10.433	2700±135.0
11.635	3000±150.0	11.234	3000±150.0	10.948	2850±142.5
45.623	14640±732.0	42.821	14850±742.5	11.501	3000±150.0
82.467	28380±1419.0	77.419	28230±1411.5	49.171	14997±749.9
106.34	38763±1938.2	100.5	38820±1941.0	82.872	27534±1376.7
124.035	48990±2449.5	124.121	51930±2596.5	107.384	37788±1889.4
–	–	–	–	130.997	50958±2547.9

Table S3. Influent and effluent concentrations of formaldehyde.

Time (h)	Ag@MWCNTs/Al_2O_3			MWCNTs/Al_2O_3		
	Degradation Rate (%)	Influent concentrations (ppm)	Enfluent concentrations (ppm)	Degradation Rate (%)	Influent concentrations (ppm)	Enfluent concentrations (ppm)
0.017	81.687	184.763	33.836	51.751	192.561	92.909
0.083	81.754	217.264	39.642	51.781	203.317	98.037
0.167	81.803	179.002	32.573	51.803	186.354	89.817
0.5	81.838	113.257	20.570	51.928	135.678	65.223
1	81.927	84.357	15.246	52.146	94.221	45.089
2	82.011	126.354	22.730	52.297	143.326	68.371
3	82.098	146.357	26.201	52.381	131.287	62.518
4	82.152	163.012	29.094	52.451	155.374	73.879
5	82.211	130.564	23.226	52.567	149.258	70.798
6	82.217	121.685	21.639	52.613	137.201	65.015
7	82.226	144.135	25.619	52.577	168.973	80.132
8	82.234	150.389	26.718	51.192	143.576	70.077
9	82.231	146.027	25.948	48.228	158.324	81.968
10	82.198	127.118	22.630	45.342	140.352	76.714
12	82.137	168.427	30.086	39.334	137.321	83.307

14	81.996	186.534	33.584	32.892	169.578	113.800
16	81.853	140.386	25.476	27.081	152.876	111.476
18	81.689	160.218	29.338	20.236	188.362	150.245
20	81.513	155.22	28.696	14.172	146.877	126.062
22	81.299	139.764	26.137	7.369	147.461	136.595
24	81.019	156.389	29.684	2.65	159.378	155.154
28	80.318	172.843	34.019	0.061	130.894	130.814
32	79.807	169.345	34.196	0.227	132.887	132.585
36	79.454	123.897	25.456	0.003	124.387	124.383
40	79.315	143.567	29.697	0	119.857	119.857
44	79.281	130.845	27.110	0	136.879	136.879
48	79.279	121.361	25.147	0	128.547	128.547

Table S4. Comparison of formaldehyde degradation of the Ag@MWCNTs/Al_2O_3 hybrid filter and other formaldehyde catalytic materials.

Sample	Formaldehyde Degradation (%)								Ref
Temperature (°C)	15	25	35	45	55	100	140	180	
Ag@MWCNTs /Al_2O_3	77.44	82.23	89.27	95.59	99.99	–	–	–	This work
Ag/Al_2O_3	–	–	< 10	< 10	< 20	–	–	–	6
Ag/TiO_2	–	–	< 10	< 15	< 40	–	–	–	6
Ag/CeO_2	–	–	< 10	< 10	< 20	–	–	–	6
Ag/MnO_x/CeO_2	–	< 30	< 30	< 40	≤ 40	–	–	–	7

Ag/SiO_2	–	–	–	–	–	< 10	≤ 50	< 95	8
$Ag/MnO_x/SiO_2$	–	–	–	–	–	< 5	< 40	100	8
Au/CeO_2	< 10	< 15	< 25	< 30	< 40	–	–	–	9
Pt/TiNT	–	–	< 60	≤ 80	< 95	–	–	–	10
Au/CeO_2-Co_3O_4	–	61	< 95	100	–	–	–	–	11
Pt/TiO_2	–	100	100	100	100	100	–	–	12
Rh/TiO_2	–	< 20	< 25	30	< 50	100	–	–	12
Au/TiO_2	–	< 5	< 10	≤ 10	< 15	< 70	–	–	12
Pd/TiO_2	–	< 5	< 10	≤ 10	< 20	< 90	–	–	12

Table S5. Amount of MWCNTs and AgNPs in sample as determined by gravimetric method.

Sample	Total Weight (g)	Amount of MWCNTs in the sample (wt%)	Amount of AgNPs in the sample (wt%)
Al_2O_3	5.1572	–	–
Al_2O_3 after acid treatment	5.1390	–	–
MWCNTs/Al_2O_3	5.1845	0.530	–
MWCNTs/Al_2O_3 after acid treatment	5.1439	0.508	–
Ag@MWCNTs/Al_2O_3; polyol reaction time of 20 min	5.1481	–	0.082
Ag@MWCNTs/Al_2O_3; polyol reaction time of 40 min	5.1532	–	0.181
Ag@MWCNTs/Al_2O_3; polyol reaction time of 60 min	5.1665	–	0.437

11. SiO_2 particle retention characterization

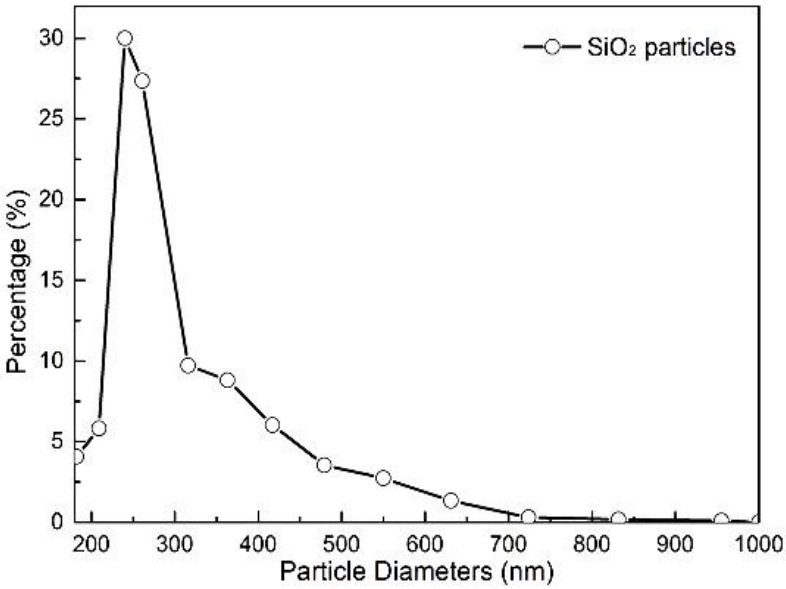

Figure S14. Particle size distribution of SiO_2 particles used in filtration test.

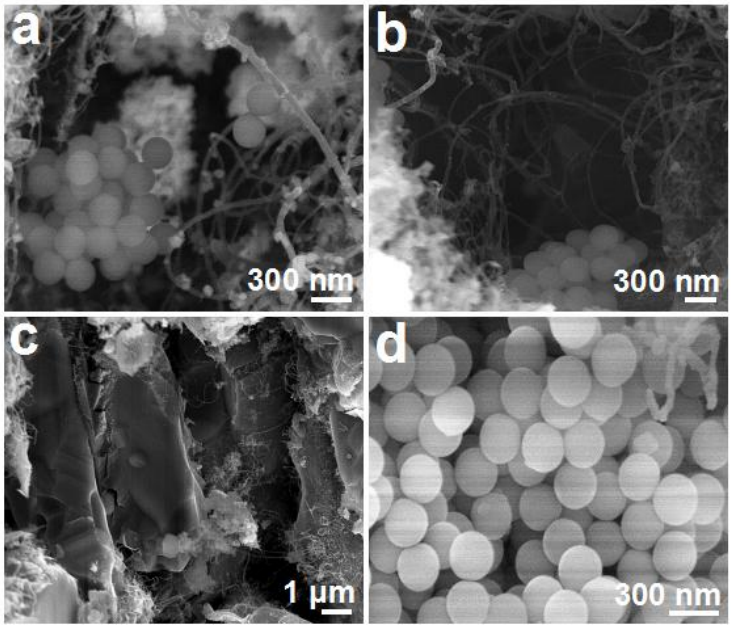

Figure S15. FESEM images of the Ag@MWCNTs/Al_2O_3 hybrid filter after gas filtration. Accumulation of the SiO_2 particles on the Ag@MWCNTs network around the pores of the Al_2O_3 filter (a,b), in the inner pore channels of the filter (c), and on the surface of the Ag@MWCNTs/Al_2O_3 hybrid filter (d).

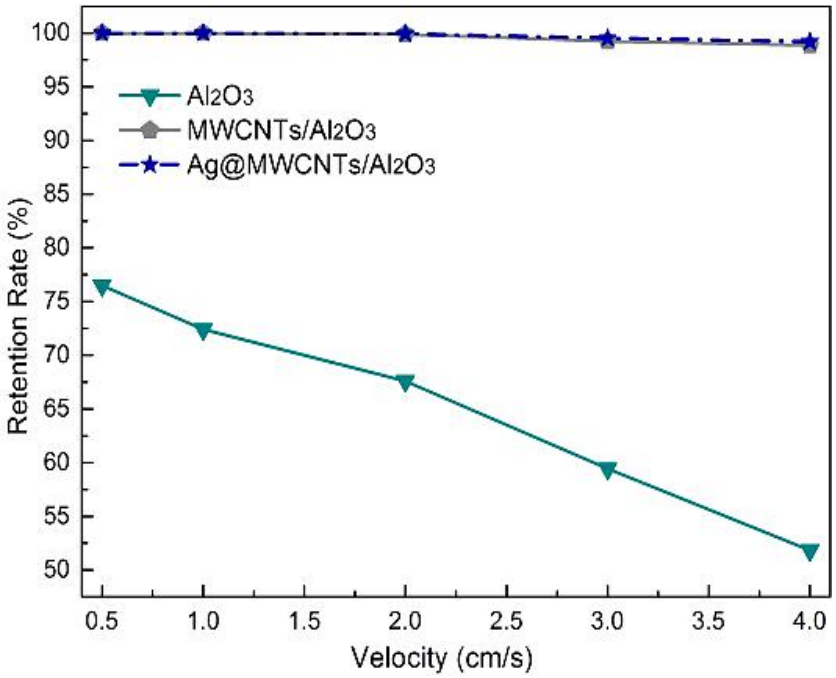

Figure S16. The relationship between the gas velocity and SiO_2 retention rate of the filters (Thickness of all filters: 1 mm).

12. Effect of loading of AgNPs

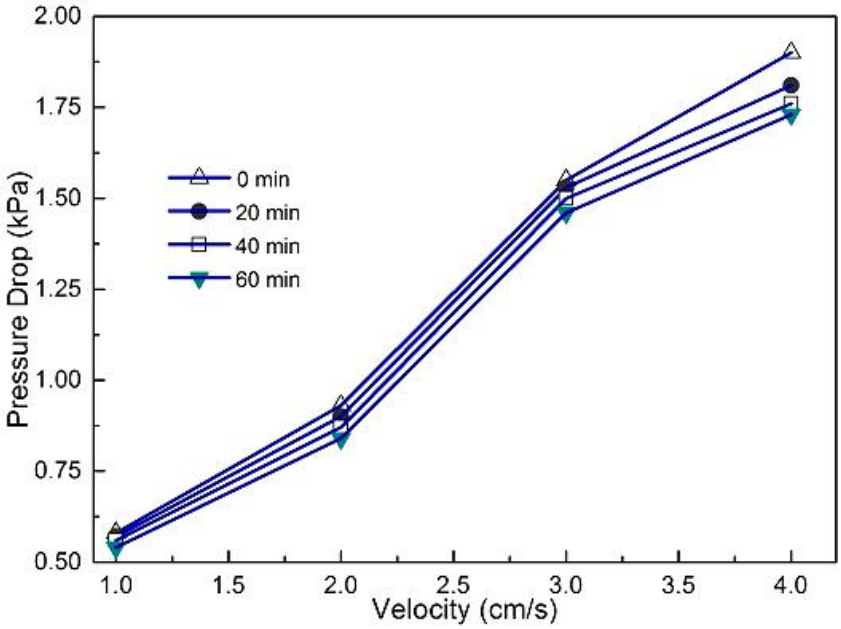

Figure S17. Pressure drop varying with gas velocity for different polyol process time of the Ag@MWCNTs/ Al_2O_3 hybrid filters.

The relationship between the gas velocity and pressure drop for different polyol process time varied from 20 min to 60 min of the Ag@MWCNTs/Al_2O_3 hybrid filters is shown in **Figure S17**. Higher loading of AgNPs in Ag@MWCNTs/Al_2O_3 hybrid filter causes the decrease of pressure drop of the filters since the "slip effect" could occur to reduce the drag force and the air flow near the Ag@MWCNTs could be in the FMF regime.[13] The Ag@MWCNTs/Al_2O_3 hybrid filter with the polyol process time of 60 min shows the lowest pressure drop at varying gas flow rate between 1.0 and 4.0 cm/s compared to the other two filters, implying that introducing the nanomaterials such as AgNPs and MWCNTs to filters could decrease the pressure drop during filtration.

13. Effect of filter thickness

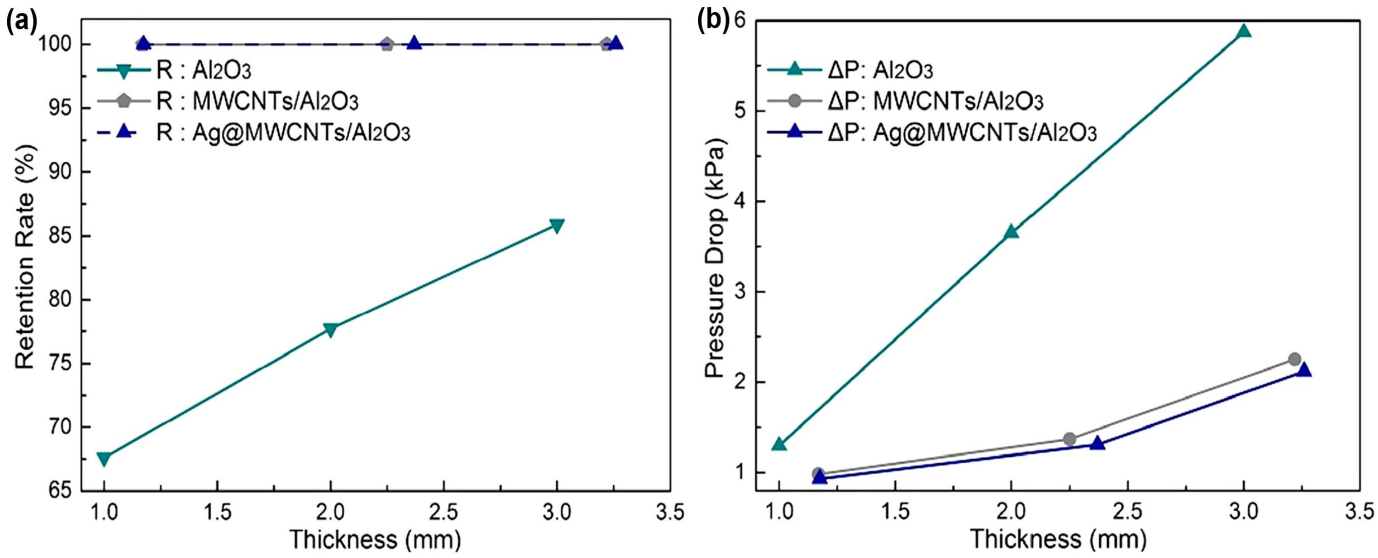

Figure S18. Retention rate (a) and pressure drop (b) of the filters varying with the filter thickness (gas velocity controlled at 2 cm/s).

References

1 T. Belin and F. Epron, *Mater. Sci. Eng., B*, 2005, **119**, 105-118.

2 C. H. Li, K. F. Yao and J. Liang, *Carbon*, 2003, **4**, 858-860.

3 Y. Zhao, Z. X. Zhong, Z. X. Low and Z. Yao, *RSC Adv.*, 2015, **5**, 91951-91959.

4 M. M. Titirici, R. J. White, N. Brun, V. L. Budarin, J. H. Clark, S. S. Dang, F. D. Monte and M. J. MacLachlan, *Chem. Rev.*, 2015, **44**, 250-290.

5 F. Alimohammadi, M. P. Gashti, A. Shamei and A. Kiumarsi, *Superlattices Microstruct.*, 2012, **52**, 50-62.

6 J. H. Zhang, Y. B. Li, Y. Zhang, M. Chen, L. Wang, C. B. Zhang and H. He, *Sci. Rep.*, 2015, **5**, 12950.

7 C. Shi, B. B. Chen, X. S. Li, M. Crocker, Y. Wang and Z. Ai-min, *Chem. Eng. J*,. 2012, **200-202**, 729-737.

8 T. Kharlamova, G. Mamontov, M. Salaev, V. Zaikovskii, G. Popova, V. Sobolev, A. Knyazev and O.Vodyankina, *Appl. Catal. A-Gen.*, 2013, **467**, 519-529.

9 J. Zhang, Y. Jin, C. Y. Li, Y. N. Shen, L. Han, ; Z. X. Hu, X. W. Di and Z. L. Liu, *Appl. Catal. B-Environ.*, 2009, **91**, 11-20.

10 H. Y. Chen, M. N. Tang, Z. B. Rui and H. B. Ji, *Ind. Eng. Chem. Res.*, 2015, **54**, 8900-8907.

11 B. C. Liu, Y. Liu, C.Y. Li, W. T. Hu, P. Jing, Q. Wang and J. Zhang, *Appl. Catal. B-Environ.*, 2012, **127**, 47-58.

12 C. B. Zhang, H. He and K. I. Tanaka, *Appl. Catal. B-Environ.*, 2006, **65**, 37-43.

13 P. Li, C. Y. Wang, Y. Y. Zhang and F. Wei, *Small*, 2014, **10**, 4543-4561.